4.13 ESTIMATES OF UPPER LEVEL TURBULENCE BASED ON SECOND ORDER STRUCTURE FUNCTIONS DERIVED FROM NUMERICAL WEATHER PREDICTION MODEL OUTPUT

Rod Frehlich* and Robert Sharman
Research Applications Program
National Center for Atmospheric Research
Boulder, CO 80307

ABSTRACT

Estimates of small-scale turbulence from numerical model output are produced from local estimates of the spatial structure functions of model variables such as velocity and temperature. The key assumptions used are the existence of a *universal* statistical description of small-scale turbulence and a locally *universal* spatial filter for the model variables. The shape of the model spatial filter is determined by comparisons with published results for the spatial structure functions derived from the GASP and MOZAIC aircraft data collected at cruising altitudes. This universal filter is used to estimate the magnitude of the small-scale turbulence, i.e., scales smaller than filter scale. A simple yet universal description of the basic statistics (such as the probability density function and the spatial correlation) of these small-scale turbulence levels in the upper troposphere and lower stratosphere is proposed. This technique can be used to diagnose and forecast upper level turbulence, and statistical evaluations of its performance in that regard are presented.

1. INTRODUCTION

Commercial, air taxi, and general aviation (GA) encounters with turbulence continue to be a source of occupant injuries, and in the case of GA, often of fatalities and loss of aircraft. According to a recent MCR Federal survey of NTSB accident data for the years 1983-1997 (Eichenbaum, 2000), turbulence contributed to 664 accidents leading to 609 fatalities (mostly GA), 239 serious and 584 minor injuries, for an estimated average annual societal cost of $134 M. Of significance here is that the MCR Federal report also estimated that *only about 30% of these upper level incidents were forecast based on previous turbulence pilot reports (PIREPs) or valid AIRMETs.* Clearly, even with this most liberal definition of a forecast, there is much room for improvement.

Theses numbers underscore the difficulties associated with forecasting turbulence, either by manual means or by automated forecasting systems. A major source of the difficulty is related to the fact that, from the meteorological perspective, turbulence is a “microscale” phenomenon. In the atmosphere, turbulent “eddies” are contained in a spectrum of sizes, from 100s of kilometers down to centimeters. But aircraft bumpiness is most pronounced when the size of the turbulent eddies encountered are about the size of the aircraft; for commercial aircraft this would be eddy dimensions of about 100m. It is impossible to directly forecast atmospheric motion at this scale, now or even in the foreseeable future. Fortunately, it appears that most of the energy associated with eddies of this scale cascades down from the larger scales of atmospheric motion (e.g. Dutton and Panofsky, 1970, Cho and Lindborg 2001), which may in fact be resolved by current weather observations and numerical weather prediction (NWP) models. Assuming the large-scale forecasts are sufficiently accurate, the turbulence forecasting problem is then one of identifying large-scale features that are conducive to the formation of aircraft scale eddies.

But when using NWP models as a basis for turbulence forecasts, it is important to realize that the smallest scales resolvable by the model (i.e., those scales closest to the scales of aircraft turbulence) are in fact underrepresented because of explicit and implicit smoothing and filtering and other underresolution effects (e.g., Frehlich and Sharman 2004). In most NWP models these effects are mostly undocumented since emphasis has traditionally been on accurate representations

* Corresponding author address: NCAR/RAP, PO Box 3000, Boulder, CO 80307. Also at University of Colorado, CIRES, UCB 216, Boulder, Co, 80309, Frehlich@ucar.edu

of the larger scale motions that contribute most significantly to meteorological phenomena, and to some extent, the need to produce numerically stable solutions rather than to describe the details of the turbulence field.

In this paper we develop methods to quantify, for certain atmospheric regimes, the effects of spatial filtering in NWP models, and consequently produce more accurate estimates of the small-scale turbulence. Here the term "small-scale" will be used to refer to the smallest resolvable scales of an atmospheric dynamical model (i.e. scales smaller than the filter scale), which with suitable extrapolation, may be used to infer the magnitude of "subgrid" scale motions as well.

The first step in the process is to assess the statistical properties of the spatial variability of the atmosphere on scales both resolvable and unresolvable by current NWP models (i.e., scales smaller than about 100 km). The most reliable statistical data available on these scales is probably the Global Atmospheric Sampling Program (GASP) (Nastrom and Gage 1985) in the US and MOSAIC (Measurements of Ozone by Airbus In-service airCraft) program in Europe (Lindborg 1999; Cho and Lindborg 2001). This data was obtained by specially instrumented commercial aircraft collecting wind and temperature data at aircraft cruise levels (approximately 8-10 km MSL, i.e., in the upper troposphere and lower stratosphere) over several thousand flight legs. The statistical analyses of these datasets demonstrated rather convincingly that the atmospheric wind and temperature spatial spectra at middle latitudes and upper levels exhibit a $k^{-5/3}$ behavior where k is the horizontal wavenumber (or equivalently exhibit an $s^{+2/3}$ behavior for the second-order structure function, where s is the separation) from scales ranging from about 400 km down to 1 km. Flights of research aircraft also show a persistent $k^{-5/3}$ scale dependence (Sharman and Frehlich 2003). An example of velocity and temperature spectra from data collected by NCAR's C130 research aircraft during the INDOEX campaign is shown in Fig. 1.

The cause of the observed $k^{-5/3}$ statistical behavior is at the moment not completely understood. Discussions of competing theories are provided, for example, by Tung and Orlando (2003), Cho and Lindborg (2001), and by Koshyk and Hamilton (2001) within the context of recent simulation results which seem to point to a downscale cascade. For our purposes, it is sufficient merely to accept the $k^{-5/3}$ spectral behavior as a universal statistical description of mid-latitude upper-level "turbulence" so that this behavior can be used as "truth" to quantify the underrepresentation of the small-scale motions in mesoscale models. Depending on the model numerics and filtering used, a mesoscale model will in general show an energy deficit from this assumed universal statistical behavior, and generally this deficit will be largest for the smallest scales resolved by the model (Frehlich and Sharman 2004; Skamarock 2004). This model-dependent deficit can be estimated from the s dependence of model-derived second order structure functions compared to the expected $s^{2/3}$ behavior. For this comparison the use of structure functions is preferred since they permit accurate measurements of turbulence over small measurement domains and are more robust compared with spectral methods which suffer from windowing and aliasing effects (Frehlich 1997; Frehlich et al. 1998, 2001). Once the spatial filter of the model has been determined, information about turbulence levels can be extrapolated to scales smaller than the model resolution to provide information about the energy content of the grid scale and sub-grid scale turbulent motions.

2. STATISTICAL DESCRIPTION OF UPPER_LEVEL TURBULENCE

We assume that the spatial statistics of upper-level turbulence can be described by spatial structure functions (Lindborg 1999) (or equivalently spatial spectra). Longitudinal and transverse second-order structure functions are defined as

$$D_{LL}(\boldsymbol{s}) = \left\langle \left[v_L(\boldsymbol{x}) - v_L(\boldsymbol{x}+\boldsymbol{s}) \right]^2 \right\rangle$$
$$D_{NN}(\boldsymbol{s}) = \left\langle \left[v_N(\boldsymbol{x}) - v_N(\boldsymbol{x}+\boldsymbol{s}) \right]^2 \right\rangle \quad (1)$$

where $v_L(x)$ and $v_N(x)$ are the velocity components along and transverse to the displacement vector $s=(x,y,z)$, respectively, and <> denotes an ensemble average. Both the GASP and MOSAIC campaigns produced essentially the same average statistics for mid-latitude upper-level turbulence. The best-fit models to the combined data sets were derived by Lindborg (1999) as

$$D_{LL}(s) = a_1 s^{2/3} + b_1 s^2 - c_1 s^2 \ln s \quad (2)$$

$$D_{NN}(s) = a_2 s^{2/3} + b_2 s^2 - c_2 s^2 \ln s \quad (3)$$

where

$a_1 \approx 0.0036\ m^{4/3}s^{-2},\ a_2 \approx 0.004\ \mathrm{m}^{4/3}\mathrm{s}^{-2},$

$b_1 \approx 2.4\mathrm{x}10^{-9}\ s^{-2}, b_2 \approx 6.5\mathrm{x}10^{-9}\ \mathrm{s}^{-2},$

$c_1 \approx 0.16\mathrm{x}10^{-9}\ s^{-2}, c_2 \approx 0.43\mathrm{x}10^{-9}\ s^{-2}.$

Note that for small spacings *s*, the first term dominates, and the structure functions recover the Kolmogorov form of fully developed 3D isotropic, in which case the turbulence intensity, as measured by the eddy dissipation rate ε, is related to D_{LL} (*s*) and D_{NN} (*s*) [Monin and Yaglom (1975) Eq. (2.17)] through

$$D_{LL}(s) = C_K\ \varepsilon^{2/3}\ s^{2/3} \approx 2\ \varepsilon^{2/3}s^{2/3} \qquad (4)$$

$$D_{NN}(s) = \frac{4}{3}C_K\ \varepsilon^{2/3}\ s^{2/3} \approx \frac{8}{3}\ \varepsilon^{2/3}s^{2/3} \qquad (5)$$

where $C_K \approx 2$ is the Kolmogorov constant. For fully-developed 2D isotropic turbulence analogous relations can be written as (Lindborg 1999)

$$D_{LL}(s) = C_K\varepsilon^{2/3}\ s^{2/3} \approx 2\ \varepsilon^{2/3}s^{2/3} \qquad (6)$$

$$D_{NN}(s) = \frac{5}{3}C_K\varepsilon^{2/3}s^{2/3} \approx \frac{10}{3}\ \varepsilon^{2/3}s^{2/3} \qquad (7)$$

where ε as used here, may not strictly satisfy the definition of 3D turbulence.

An empirical function $D_{\mathrm{model}}(s)$ for the model-derived structure functions can be determined to explicitly account for the model-dependent filter function. The simplest such empirical function has the form

$$D_{\mathrm{model}}\ (s) = K\ D_{\mathrm{cor}}\ (s)\ D_{\mathrm{ref}}\ (s) \qquad (8)$$

where *K* is a constant and $D_{\mathrm{cor}}\ (s)$ describes the correction produced by the model filter, and $D_{\mathrm{ref}}(s)$ is a normalized form of the in-situ measured structure functions, e.g., the Lindborg model. Note that according to the analysis of the GASP data by Nastrom and Gage (1985) and of the MOZAIC data by Cho and Lindborg (2001), the reference structure function model depends weakly on the measurement region, i.e., altitude, latitude, and longitude, but this effect will be ignored here. If the reference normalized longitudinal structure function is taken as the Lindborg best-fit model Eq. (2), i.e.,

$$D_{\mathrm{LLref}}\ (s) = s^{2/3} + \frac{b_1}{a_1}s^2 - \frac{c_1}{a_1}\ s^2\ \ln s \qquad (9)$$

then the correction function $D_{\mathrm{cor}}(s)$ should approach unity for large separations where the effects of the spatial filter are negligible. For small spacings s, the model structure function $D_{\mathrm{model}}(s)$ should approach s^2 to reflect the spatial smoothing of the fields at the smallest scales. Therefore, we select the following simple empirical function which satisfies both these requirements

$$D_{\mathrm{LLcor}}(s) = \frac{(s/p_1)^{4/3}}{1+(s/p_1)^{4/3}+p_2(s/p_1)^{2/3}} \qquad (10)$$

where p_1 is the length scale of the model filter and p_2 is a fitting parameter. The best-fit constant

$$K = C_K\ \varepsilon^{2/3} \approx 2\ \varepsilon^{2/3} \qquad (11)$$

provides an estimate of ε. Alternatively, if the reference normalized transverse structure function is taken as the Lindborg 2D isotropic model

$$D_{\mathrm{NNref}}\ (s) = s^{2/3} + d_1\ s^2 - d_2 s^2 \ln s \qquad (12)$$

where $d_1=(9b_1-3c_1)/(5a_1)$, $d_2=9c_1/(5a_1)$ and the best-fit constant

$$K = \frac{5}{3}C_K\ \varepsilon^{2/3} \approx \frac{10}{3}\ \varepsilon^{2/3} \qquad (13)$$

provides an estimate of ε. The unknown parameters p_1 and p_2 are determined by minimizing the chi-squared error (Press et al. 1986) between the empirical model and the average structure functions derived from the NWP model. For example, Fig. 2 shows the velocity structure functions derived from RUC20 NWP analyses (Benjamin et al. 2004). The same analyses on the RUC20 forecasts produce almost identical results. Note that the best-fit model structure function is almost identical to the measured structure function. Also shown in Fig. 2 is the theoretical calculation of the longitudinal (LL60 km) and transverse (NN60 km) structure functions assuming the model values are given by a 60 km grid cell and assuming the atmospheric statistics are described by the 2D isotropic Lindborg. As can be seen, the RUC20 analysis is

well approximated by the 60 km grid cell filtering for the longitudinal structure function while there is a small error for the transverse structure function. This heavy filtering is typical of NWP models.

The RUC20 model also provides diagnostic estimates of the vertical velocity *w* (related to the vertical *p* velocity ω) and should also contain information about the small-scale turbulence. Unfortunately, *in situ* truth measurements of vertical velocity statistics are not available from aircraft data as they are from the GASP and MOZAIC data for horizontal velocities, however, a simple model is provided from turbulence theory. We propose a universal model for the structure function of the RUC20 *w* field as

$$D_{\text{model}}(s) = \frac{K(s/c_1)^{c_2}}{1+(s/c_1)^{c_2}+c_3(s/c_1)^{c_4}} \qquad (14)$$

where

$$K = 2\sigma_w^2 \qquad (15)$$

and σ_w^2 is the variance of the vertical velocity. The yearly average of the RUC20 *w* structure function analyses at 10 km altitude and the best fit model is shown in Fig. 3 with the characteristic constant value of $K=2\sigma_w^2$ at large lags indicating uncorrelated vertical velocity fluctuations.

3. ESTIMATES OF LOCAL TURBULENCE INTENSITY

Various methods have been proposed to estimate turbulence associated with unresolved scales (i.e., subgrid scale or sgs) from resolved scales of the numerical model fields. The most common are based on prognostic equations of the sgs turbulent kinetic energy (TKE) (e.g., Deardorff 1970; Moeng and Sullivan 1994; Pielke 2002). This requires assumptions about the local conditions to connect resolved scale gradients to sgs TKE. Since the horizontal statistics of the velocity and temperature fields have a robust description, we propose instead to estimate local (i.e., all scales less than the model filter cutoff, including subgrid scales) turbulence intensities based on the assumption of a universal spatial filter for the model as outlined in the previous section. A similar approach has been used to estimate the statistics of small-scale turbulence from lidar measurements using a correction for the spatial average of the lidar pulse (Frehlich 1997; Frehlich et al. 1998; Frehlich and Cornman 2002). If the model does indeed have a universal filter function, i.e., the functional form of the structure functions is independent of location, then local estimates of the level *K* (or equivalently of $\varepsilon^{2/3}$ or $2\sigma_w^2$) can be produced by a best-fit to the shape of the structure functions using the previously derived longitudinal and transverse structure functions, respectively (Frehlich and Sharman 2004). For the horizontal velocities the longitudinal structure functions seem to have a slightly better defined $s^{2/3}$ region (cf. Fig. 2), so we use the average of the two longitudinal structure functions (east-west and north-south) to produce local estimates of ε. In Fig. 4 plots are provided of average longitudinal structure functions of horizontal velocity at various locations in a RUC20 model field at an altitude of 10 km and the corresponding estimates of $\varepsilon^{1/3}$ derived from a 5x5 point horizontal domain (100x100 km). Note that at each location the fit is quite good, and the shape of the structure functions is approximately the same, but the levels $\varepsilon^{1/3}$ can differ considerably.

In a similar manner, local estimates of the turbulence intensity σ_w can be produced from the best-fit constant *K* to the structure functions of *w*. Examples of a few structure functions and the corresponding estimates of σ_w are shown in Fig. 5. Note that the *w* structure functions have more variability than the structure functions of horizontal velocity shown in of Fig. 4.

4. ESTIMATES OF THE PROBABILITY DENSITY FUNCTION OF LOCAL TURBULENCE

The statistical description of the structure function estimates of the local turbulence levels ε or σ_w is fully described by the probability density function (PDF). The PDF of the variations in the spectral level of the GASP data is well described by a log-normal distribution (Nastrom and Gage 1985). This is equivalent to a log-normal PDF for ε, which is completely defined by the two parameters: $\langle \log \varepsilon \rangle$ or the median value ε_{50} and the standard deviation $\sigma_{\log\varepsilon}$ of $\log_{10}\varepsilon$. From the GASP data, Frehlich (2001) derived these parameters as $\varepsilon_{50}=2.66\text{x}10^{-5}\text{m}^2\text{s}^{-3}$, $\sigma_{\log\varepsilon}=0.63$, and in addition, $\langle\varepsilon\rangle=7.64\text{x}10^{-5}\ \text{m}^2\text{s}^{-3}$. The PDF of the RUC20 estimates of ε from local structure function estimates over an *L*x*L* sub-domain for two values of *L* are compared to the log-normal

model with these parameters in Fig. 6. It should be pointed out that the estimates of ε from the GASP data were produced from the spectral level at a wavelength of 400 km for flight legs longer than 2400 km (i.e., *along a line*) which will have different statistics than the RUC20 estimates which were produced *over a square domain* (see Frehlich and Sharman 2004). However, all the PDFs agree well with the log-normal model, although the RUC20 derived estimates depend on the averaging length *L*.

5. THE USE OF STRUCTURE FUNCTION ANALYSES TO DIAGNOSE UPPER- AND MID-LEVEL TURBULENCE CONDITIONS

Over the years there have been continuous efforts to nowcast and forecast the occurrence aircraft-scale turbulence through the use of various manual and automated turbulence diagnostics derived from NWP model output (e.g., Ellrod and Knapp 1992, Marroquin 1998, Tebaldi et al., 2002). Most of these turbulence diagnostics do not have a rigorous basis from turbulence theory, but rather relate expected turbulence intensities to larger scale features in the atmosphere, such as upper-level fronts and jet streams. However, we can apply the ideas presented in the previous sections to use NWP model-derived structure functions to produce patterns of turbulence intensities $\varepsilon^{1/3}$ and σ_w as shown in the example of Fig. 7. These contours were produced from a particular RUC20 analysis at 10 km. Note the high spatial variability in both fields. For reference Fig . 8 shows the associated synoptic situation. It is apparent in this and other cases we've looked at, that large values of $\varepsilon^{1/3}$ correlate well with large shears that may be associated with an upper level jet for example, but the larger values of σ_w seem to correspond to regions of convective activity. This these two diagnostics seem to be identifying different turbulence sources.

Currently, the accuracy of the derived values of $\varepsilon^{1/3}$ and σ_w (or any other turbulence diagnostic) can be assessed from the only routine observations of atmospheric turbulence available, reports of encounters with turbulence by pilots (PIREPs). PIREPs are semi-automated and give information about a turbulence encounter (time, latitude, longitude, altitude, severity), however there is some subjectivity associated with these reports, especially with regard to severity (reported on a 5 point scale: null, light, moderate, severe, or extreme), and it must be realized that the report is based on a turbulence experience along a flight path, i.e. along a line. If the model-derived diagnostics are supposed to be a grid point average, the correspondence to a line is not necessary direct. Nevertheless, the relative performance of various diagnostics can be evaluated by comparisons to turbulence PIREPs as in Tebaldi et al. (2002). In that study the metric used to evaluate the performance of various turbulence diagnostics was the area contained under probability of detection (POD) curves, similar to radar operating characteristic curves.

To construct POD curves, a set of thresholds are assumed for each diagnostic, and given that threshold, the diagnostic performance based on comparisons to available turbulence pilot reports was evaluated for both null (as measured by PODN, the fraction of null events correctly detected) and moderate or greater turbulence reports (as measured by PODY, the fraction of moderate or greater turbulence events correctly detected). The curves are then produced from the computed PODY values versus PODN values for each of the chosen thresholds. For small values of the chosen threshold, PODY will obviously be high, near unity, while PODN will be low, near 0, and vice versa for large values of the chosen threshold. For the range of thresholds selected, higher combinations of PODY and PODN and therefore larger areas under the PODY-PODN curves, imply greater skill in discriminating between null and moderate-or-greater turbulence events. Uncorrelated diagnostics produce a straight diagonal line indicating no skill.

Figs. 9 and 10 show POD curves constructed in this manner for the $\varepsilon^{1/3}$ and σ_w diagnostics based on structure function computations for upper- and mid-levels respectively, compared to the Marroquin (1998) TKE diagnostic. The Marroquin (1998) approach uses a steady state approximation to the TKE prognostic equation, and should therefore provide similar estimates of TKE to those produced by most sub-grid parameterizations used in current NWP models. The diagnostics were computed from RUC20 1800 UTC 6-hour forecasts (valid at 0000 UTC) analyses over a 3-month period from Nov 2002-Jan 2003. Based on the area under the curves, the structure function derived $\varepsilon^{1/3}$ and σ_w diagnostics are superior to TKE diagnostic. These algorithms are therefore potentially quite useful for operational forecasting of upper-level and mid-level turbulence, and the optimal combination of all the diagnostic metrics is currently being evaluated.

6. DISCUSSION

A procedure has been presented to estimate the small-scale turbulence levels from any mesoscale NWP model using estimates of the local structure functions of model variables, provided adequate spatial resolution is available to resolve at least part of the $s^{+2/3}$ (or $k^{-5/3}$) power-law region. The key assumptions for a given altitude of interest are the existence of (1) a universal statistical description of the small-scale turbulence, and (2) a universal representation of the spatial filter for the model. The extensive archive of in-situ aircraft measurements provided by the GASP and MOZAIC datasets has produced a robust universal description of the velocity and temperature fields at typical aircraft cruising altitudes of 10 km. This description is duplicated by the average structure functions derived from the RUC20 mesoscale NWP model (Fig. 2). An accurate estimate of the spatial filter of meso-scale models such as RUC20 is produced from the average structure functions of the model variables and the universal in-situ model (Fig. 2). The average velocity structure functions derived from RUC20 analyses agree well with the theoretical calculation assuming the model values are produced as an average over a 60x60 km grid cell (Fig. 2), thus indicating the true spatial filtering of the model and producing a quantitative metric for model resolution. Estimates of small-scale turbulence are produced from the scaling constant of the best-fit universal structure function to the local structure function estimates (e.g., Figs. 4, 5). These techniques could be applied to other levels (i.e., lower to mid-troposphere and stratosphere) if suitable estimates of the spatial statistics become available, either from data or reliable numerical simulation models. To produce the mid-level POD plots presented in Fig. 11 an atmospheric statistical description of Lindborg (1999) is assumed to apply.

The climatology of the small-scale turbulence is well defined by the probability density function (PDF) and the spatial statistics of the estimates. The PDF of small-scale turbulence levels for the velocity field described by ε (Fig. 6) is approximately log-normal, i.e., the $\log_{10}$ of ε has a normal or Gaussian distribution. However, the parameters of the log-normal distribution depend on the averaging length L and have simple scaling laws (Frehlich and Sharman 2004). The variability of the small-scale metrics for turbulence intensity is the essential component of Kolmogorov's refined similarity theory (Monin and Yaglom 1975) for velocity fields and the extension to the temperature field. An accurate statistical description of atmospheric turbulence must include this variability.

There are many applications for these local turbulence estimates. These include incorporating the turbulence related variability into optimal data assimilation methods, improving subgrid scale turbulence parameterizations, forecasting turbulence and climatology of aircraft-scale turbulence for aviation safety, extracting turbulence climatologies from archived model fields, and calculating accurate error bars for various statistics.

With regards to producing turbulence forecasts, the ability to provide accurate aircraft scale turbulence nowcasts and forecasts is hampered by several fundamental difficulties:

(1) The resolution of current NWP models (several 10s km to 100 km roughly) is about two orders of magnitude too coarse to resolve aircraft scale turbulence (roughly 100s m). Therefore, aircraft scale turbulence diagnoses and predictions must be based on large scale features.

(2) The performance of turbulence diagnostics is hampered by our current lack of understanding of the linkage between NWP observable scale features and aircraft scale turbulence. An implicit assumption in all current turbulence diagnostics is that turbulence generating mechanisms have their origin at resolvable scales and the energy introduced at those scales cascades down to aircraft scales, but it is unclear what the exact mechanism is that creates small scale motion from the larger scales. For example the two small-scale turbulence metrics from the RUC20 analysis $\varepsilon^{1/3}$ and σ_w have different spatial patterns as shown in Figs. 7-8. This may indicate that each metric is sensitive to different turbulence phenomena, e.g., $\varepsilon^{1/3}$ may indicate the presence of fronts and horizontal wind shears, while σ_w may be indicative of vertical variability due to large convective complexes.

(3) Even if it is true that aircraft scale turbulence has its origins at the resolvable scales, the turbulence forecast system has all the inherent NWP errors associated with the resolvable scales.

(4) It is not clear that any single turbulence diagnostic is capable of capturing all the relevant information that the larger scale representations can provide.

(5) The large amount of spatial filtering in operational NWP models may be limiting the useful information necessary to correctly diagnose the smallest scales in the model. Next generation NWP models should attempt to reduce the filtering with improved higher order numerics (e.g., Skamarock 2004).

(6) Finally, there is the difficult matter of verification. Here we have used PIREPs for statistical tuning and verification of the structure function diagnostics. But an individual PIREP is subject to spatial and temporal errors, and is subjective in its intensity rating. Since turbulence structures by their very nature are highly spatially variable (see Figs. 7-8), new verification metrics based on probabilistic forecast metrics may be required to accurately reflect the improvements in turbulence diagnostics and in the use of higher resolution models. The quantitative automated in-situ turbulence reporting system (Cornman et al., 1995) should eliminate most of the uncertainty associated with PIREPs but a link must first be established between median statistics and line average statistics for rigorous analysis.

Acknowledgments. This research is in response to requirements and funding by the Federal Aviation Administration (FAA). The views expressed are those of the authors and do not necessarily represent the official policy or position of the FAA.

REFERENCES

Benjamin, S.G., G.A. Grell, J.M. Brown, T.G. Smirnova, and R. Bleck, 2004: Mesoscale weather prediction with the RUC hybrid isentropic-terrain-following coordinate model. *Mon. Wea. Rev.*, **132,** 473-494.

Cho, J. Y. N. and E. Lindborg, 2001: Horizontal velocity structure functions in the upper troposphere and lower stratosphere 1. Observations. *J. Geophys. Res*., **106**, 10,223-10,232.

Cornman, L. B., C. S. Morse, and G. Cunning, 1995: Real-time estimation of atmospheric turbulence severity from in-situ aircraft measurements. *J. Aircraft*, **32,** 171-177.

Deardorff, J. W., 1970: A numerical study of three-dimensional turbulent channel flow at large Reynolds numbers. *J. Fluid Mech*., **41**, 453-480.

Dutton, J. and H. A. Panofsky, 1970: Clear Air Turbulence: A mystery may be unfolding. *Science*, **167**, 937-944.

Eichenbaum, H., 2000: Historical overview of turbulence accidents. MCR Federal, Inc. report TR-7100/023-1.

Ellrod, G. P. and D. L. Knapp, 1992: An objective clear-air turbulence forecasting technique: verification and operational use. *Wea. Forecasting*, **7**, 150-165.

Frehlich, R., 1997: Effects of wind turbulence on coherent Doppler lidar performance. *J. Atmos. Oceanic Technol.*, **14**, 54-75.

Frehlich, R., S. Hannon, and S. Henderson, 1998: Coherent Doppler lidar measurements of wind field statistics. *Bound.-Layer Meteor.*, **86**, 233-256.

Frehlich, R., L. Cornman, and R. Sharman, 2001: Simulation of three dimensional turbulent velocity fields. *J. Appl. Meteor*., **40**, 246-258.

Frehlich, R., and L. Cornman, 2002: Estimating spatial velocity statistics with coherent Doppler lidar*. J. Atmos. Ocean. Tech.*, **19**, 355-366.

Frehlich, R. and R. Sharman, 2004: Estimates of turbulence from numerical weather prediction model output with applications to turbulence diagnosis and data assimilation. *Mon. Wea. Rev*., in press.

Koshyk, J. N., and K. Hamilton, 2001: The horizontal energy spectrum and spectral budget simulated by a high-resolution troposphere-stratosphere-mesosphere GCM. *J. Atmos. Sci.,**58,** 329-348.*

Lindborg, E., 1999: Can the atmospheric kinetic energy spectrum be explained by two-dimensional turbulence? *J. Fluid Mech.*, **388**, 259-288.

Marroquin, A., 1998: An advanced algorithm to diagnose atmospheric turbulence using numerical model output. Preprints, *Sixteenth Conf. on Weather Analysis and Forecasting*, 79-81. Phoenix, AZ. American Meteorological Society.

Moeng, C.-H., and P. P. Sullivan, 1994: A comparison of shear- and buoyancy-driven planetary boundary layer flows. *J. Atmos. Sci*., **51**, 999-1022.

Monin, A. S., and A. M. Yaglom, 1975: *Statistical Fluid Mechanics: Mechanics of Turbulence, Volume 2*, MIT Press, 874 pg.

Nastrom, G. D., and K. S. Gage, 1985: A climatology of atmospheric wavenumber spectra

of wind and temperature observed by commercial aircraft. *J. Atmos. Sci*., **42**, 950-960.

Pielke, Roger A. Sr., 2002*: Mesoscale Meteorological Modeling*, Academic Press, 676 pp.

Press, W. H., B. P. Flannery, S. A. Teukolsky, and W. T. Vetterling, 1986: *Numerical Recipes, The art of scientific computing.* Cambridge University Press, 963 pp.

Skamarock, W. C., 2004: Evaluating Mesoscale NWP Models Using Kinetic Energy Spectra. *Mon. Wea. Rev*., in press.

Sharman, R., and R. Frehlich, 2003: Aircraft scale turbulence isotropy derived from measurements and simulations. *AIAA 2003-194*, 6-9 Jan., Reno, Nevada.

Tebaldi, C., D. Nychka, B. G. Brown, and R. Sharman, 2002: Flexible discriminant techniques for forecasting clear-air turbulence. *Environmetrics 2002*, **13**, 859-878.

Tung, K. K. and W. W. Orlando, 2003: The k^{-3} and $k^{-5/3}$ energy spectrum of atmospheric turbulence: quasigeostrophic two-level model simulation. *J. Atmos. Sci*., **60**, 824-835.

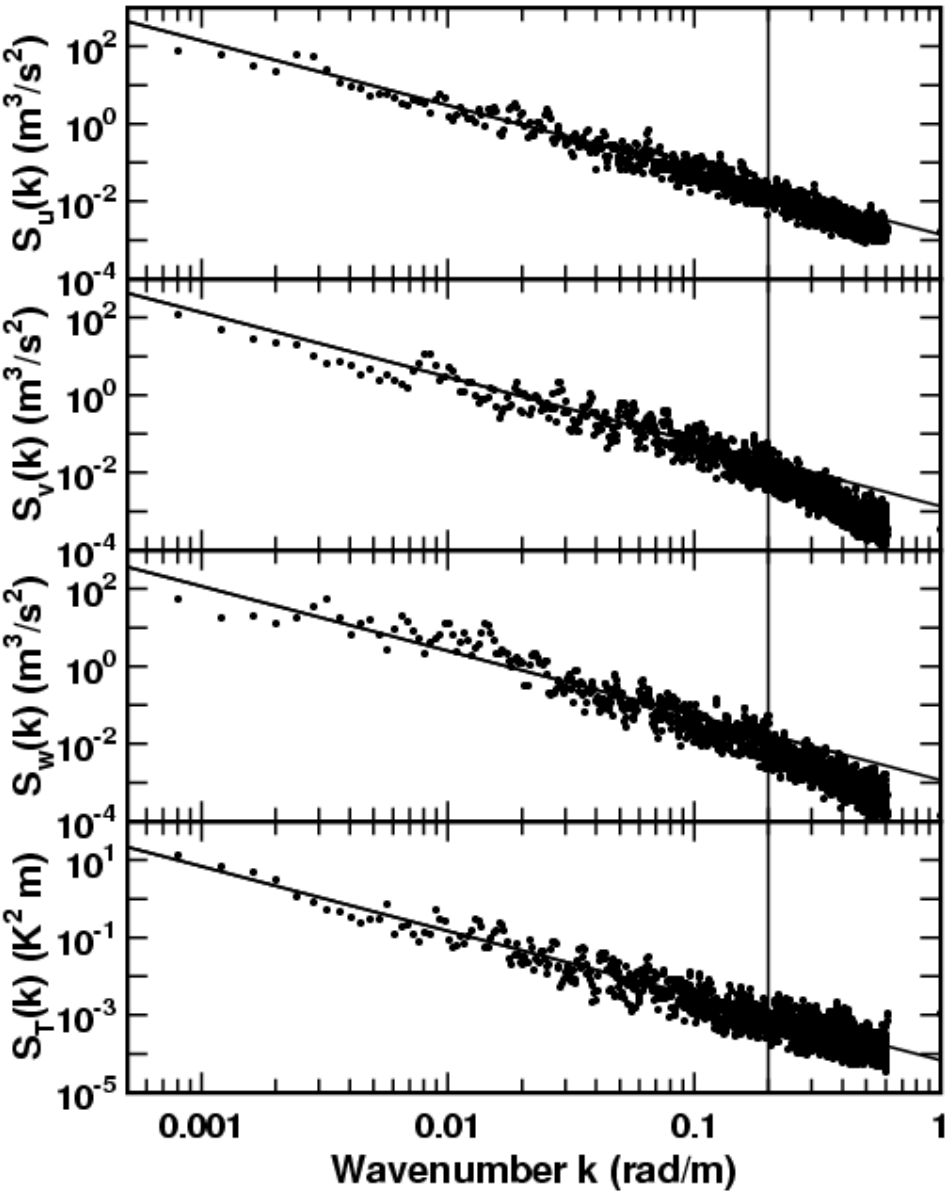

Figure 1. Longitudinal, transverse, vertical velocity, and temperature spectra, denoted $S_u(k)$, $S_v(k)$, $S_w(k)$, $S_T(k)$ respectively, as derived from INDOEX field campaign data and the best-fit Kolmogorov slope of –5/3.

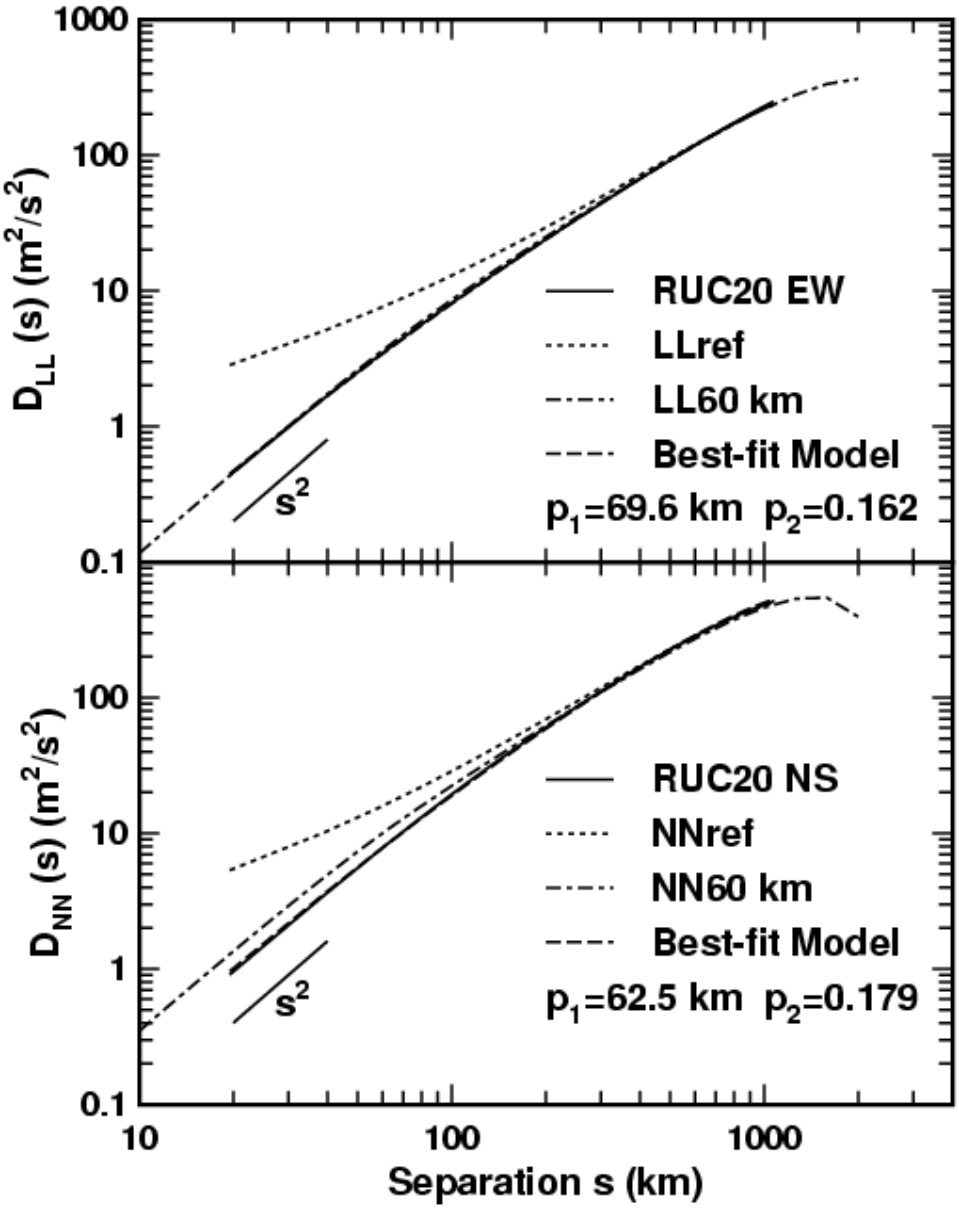

Figure 2. Average horizontal velocity structure functions from RUC20 (solid lines) for the longitudinal velocity in the East-West (EW) direction and the transverse velocity in the North-South (NS) direction, the best-fit model Eq. (8), (dashed line) with parameters p_1 and p_2, the best-fit reference models Eqs. (9) and (12) (dotted line), the theoretical predictions for a 60 km grid cell (dash dotted line), and the s^2 scaling.

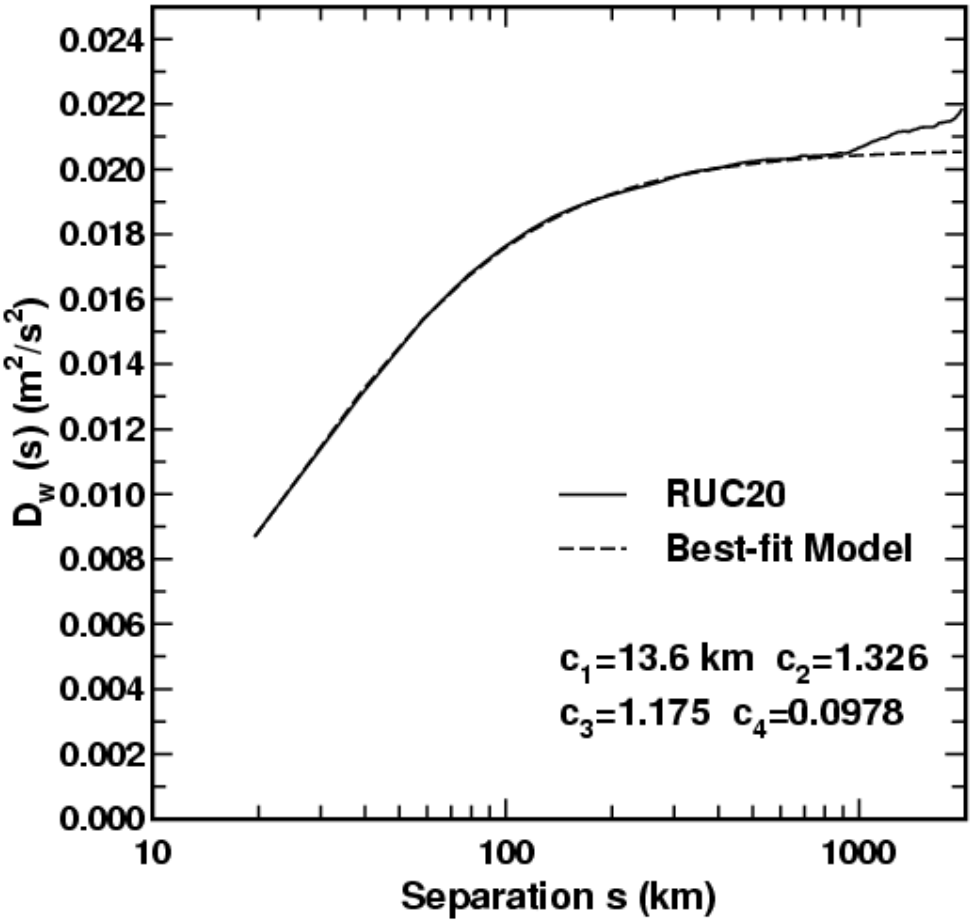

Figure 3. Average horizontal structure functions from RUC20 (solid lines) for the vertical velocity *w*, and the best-fit model Eq. (14) (dashed line) with parameters c_1 - c_4 .

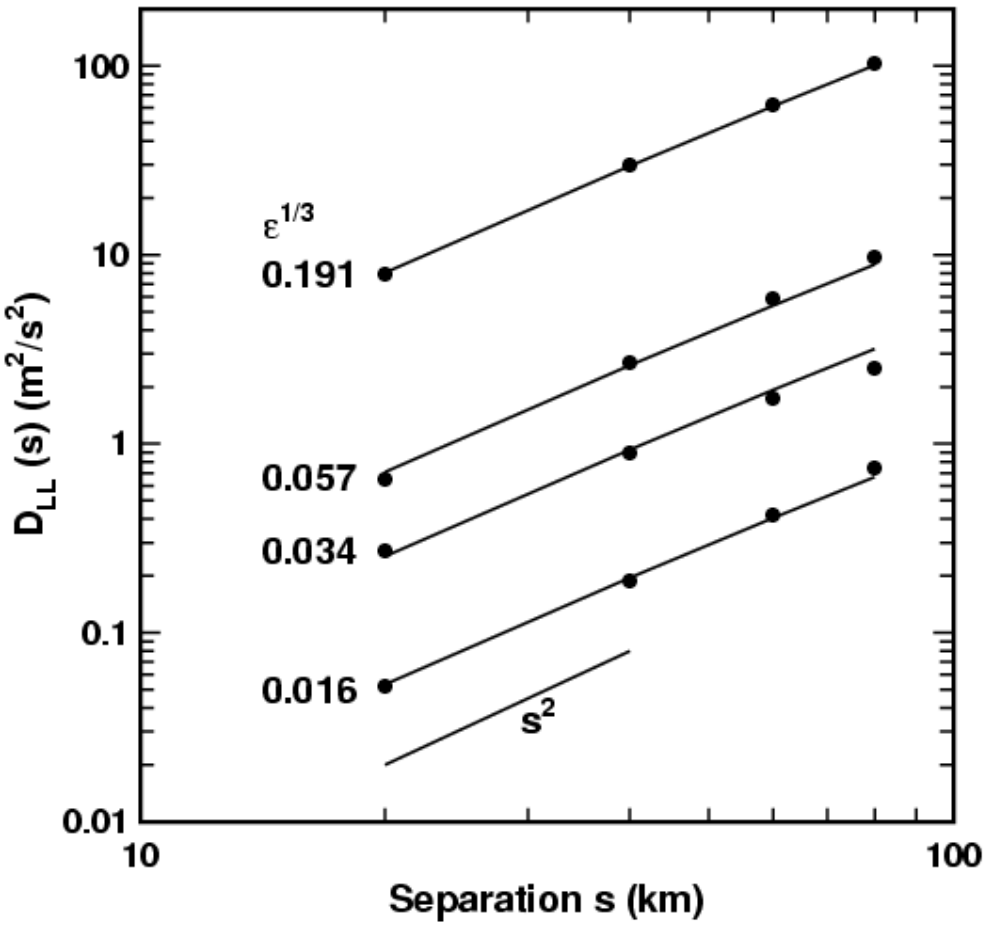

Figure 4. Example estimates (•) of longitudinal horizontal velocity structure functions $D_{LL}(s)$ from the RUC20 model using 100x100 km sub-domains, the best-fit Lindborg model Eqs. (8)-(10) (lines) with turbulence estimates $\varepsilon^{1/3}$ ($m^{2/3}s^{-1}$) from Eq. (11) given to the left of each line, and the s^2 scaling for reference.

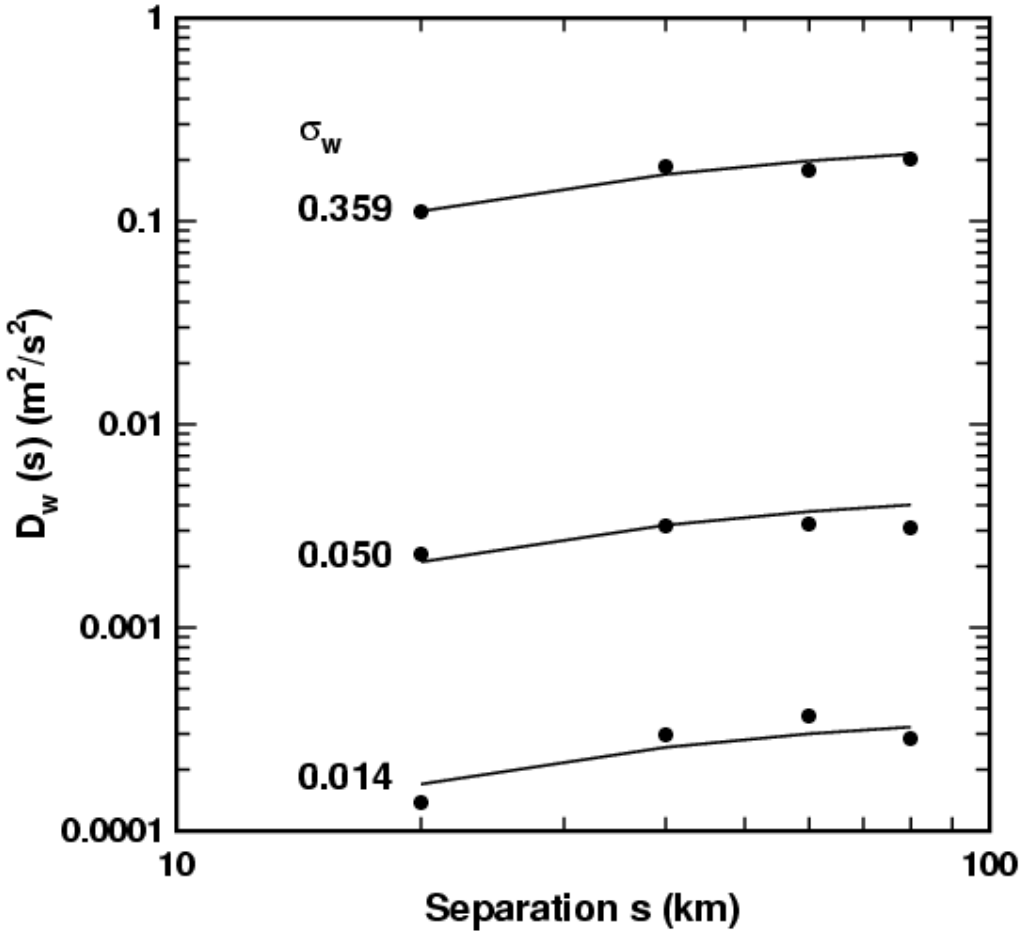

Figure 5. Example estimates (•) of vertical velocity structure functions $D_w(s)$ from the RUC20 model using 100x100 km sub-domains, the best-fit model Eq. (14) (lines) with turbulence estimates σ_w (m s^{-1}) from Eq. (15) displayed to the left of each line.

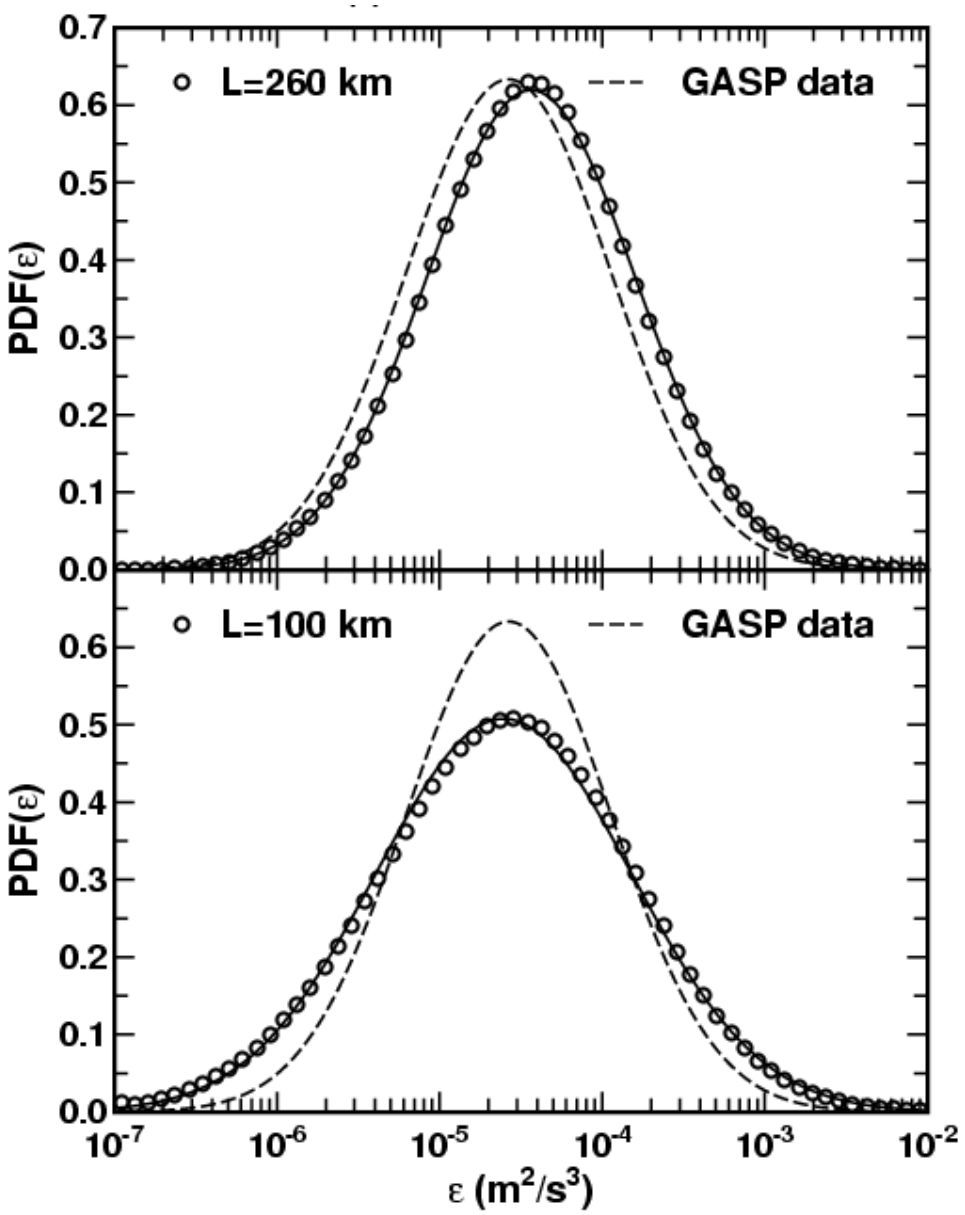

Figure 6. PDF of RUC20 estimates of ε (o) from two different square sub-domains *L*x*L*, the log-normal model prediction based on the mean and standard deviation of log ε values (solid line), and the log-normal model prediction from the GASP data derived by Frehlich (2001) (dashed line).

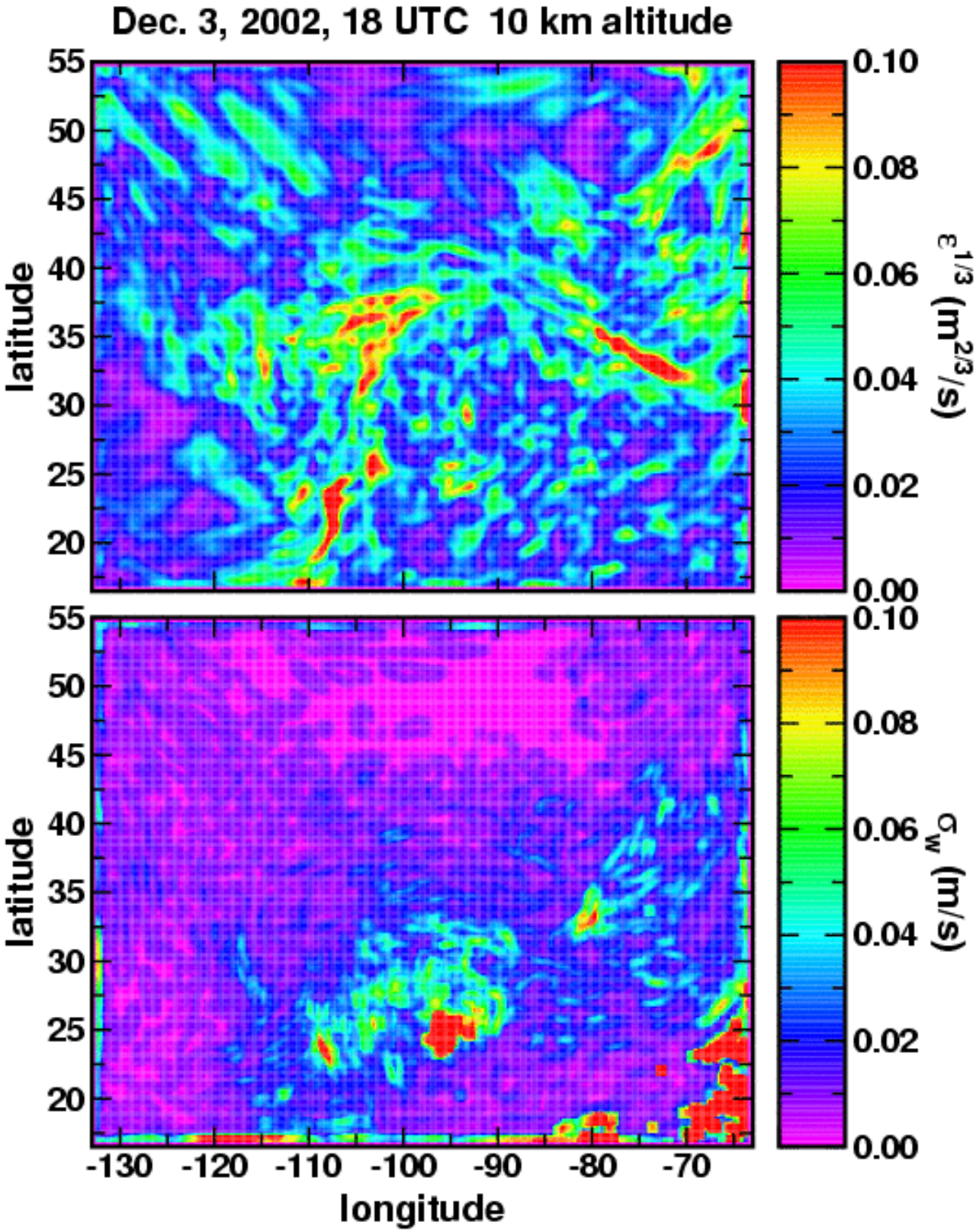

Figure 7. Estimates of small-scale turbulence $\varepsilon^{1/3}$ (upper panel) and σ_w (lower panel) for a 100x100 km measurement domain.

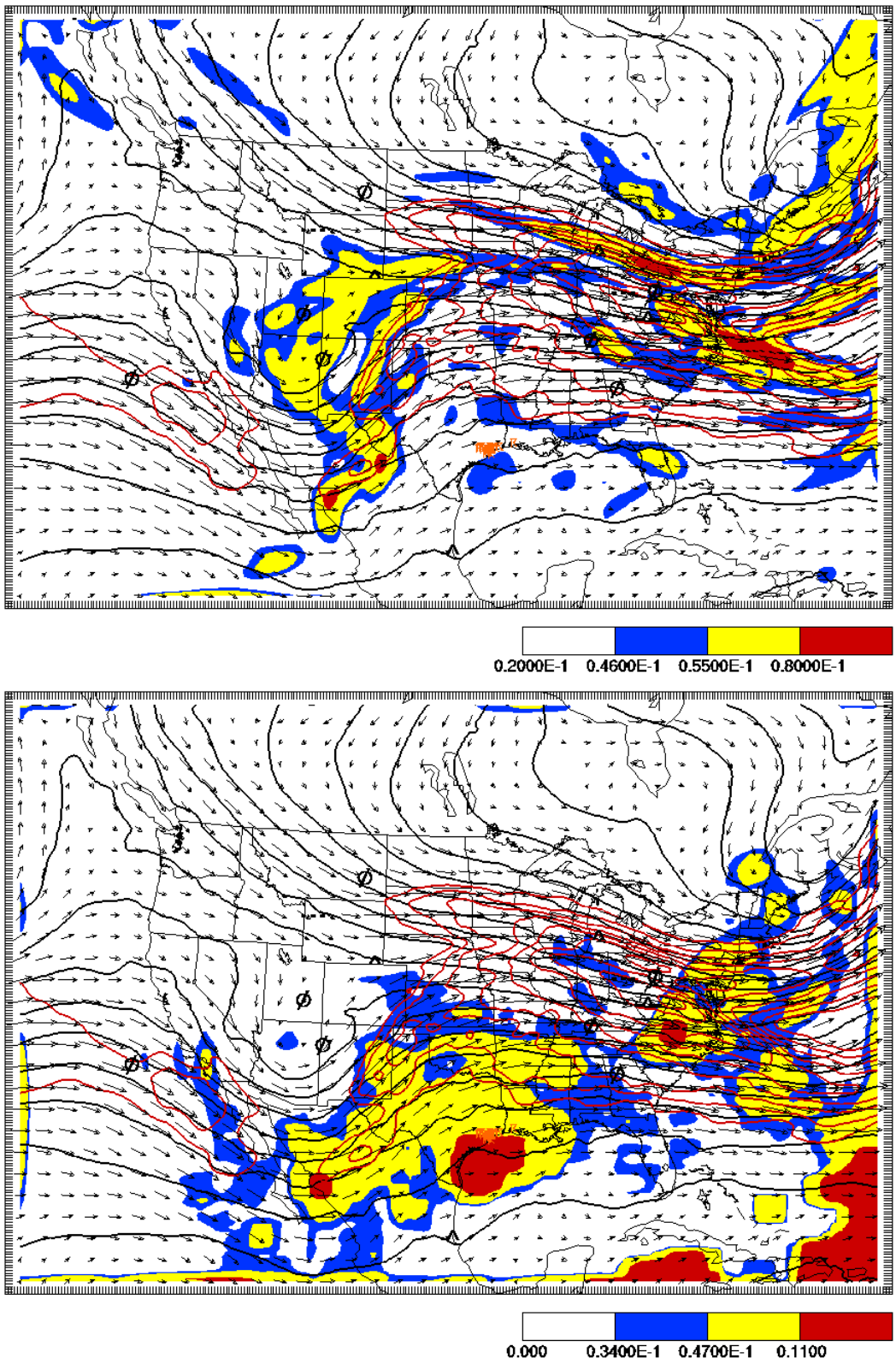

Figure 8. Contours of small-scale turbulence $\varepsilon^{1/3}$ (upper panel) and σ_w (lower panel) for a 100x100 km measurement domain for the same day/time and flight level (FL330) as Fig. 7. Solid black lines are height contours, red lines are wind speed contours > 40 m/s. Wind vectors, PIREPs, and cloud-ground lightning flashes (orange) are also shown. Note that large values of $\varepsilon^{1/3}$ correlate with the large shears associated with the upper level jet, but the largest values of σ_w correspond to regions of convective activity over southern Texas.

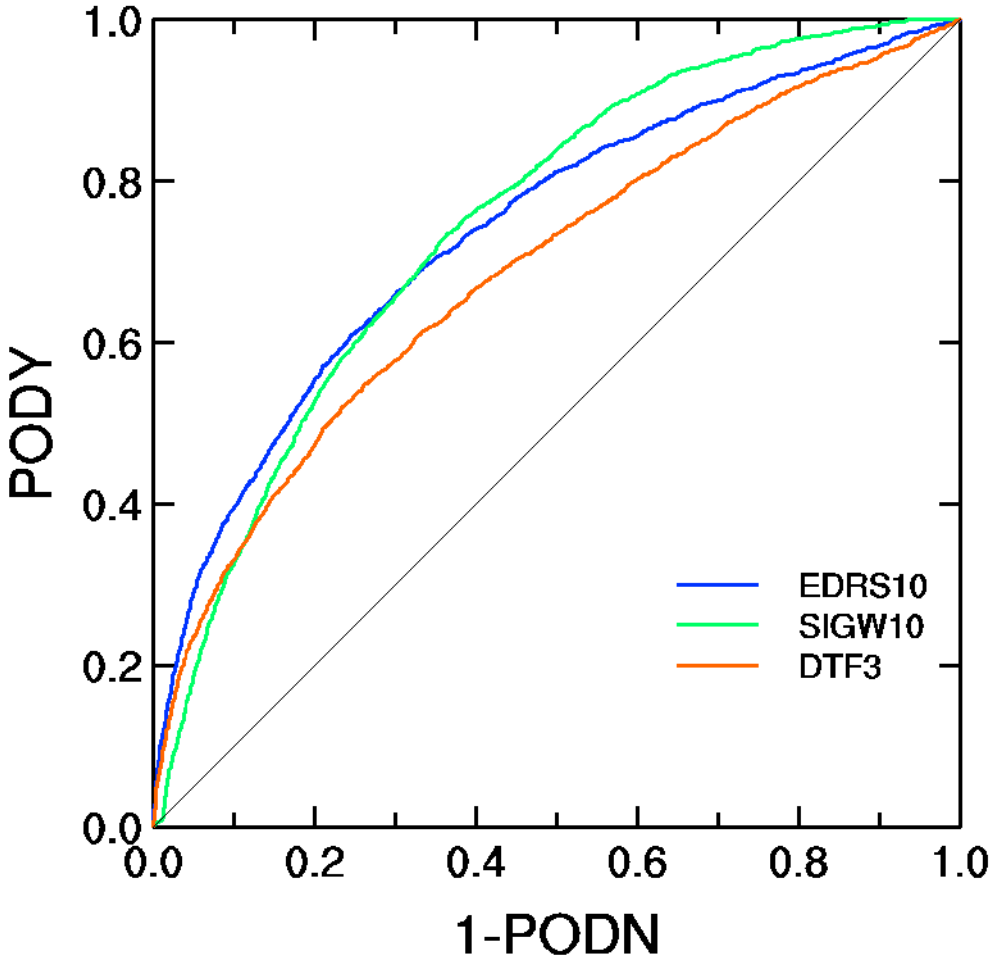

Figure 9. The probability of a (moderate-or-greater) turbulence detection PODY vs the probability of no turbulence PODN from RU20 structure function derived turbulence estimates $\varepsilon^{1/3}$ (blue curve) and σ_w (green curve) compared to the Marroquin TKE diagnostic (orange curve). The case of no skill is also shown as a light diagonal line. The curves are based on 14,614 PIREPs collected at upper levels (FL>200) over a 3-month winter period.

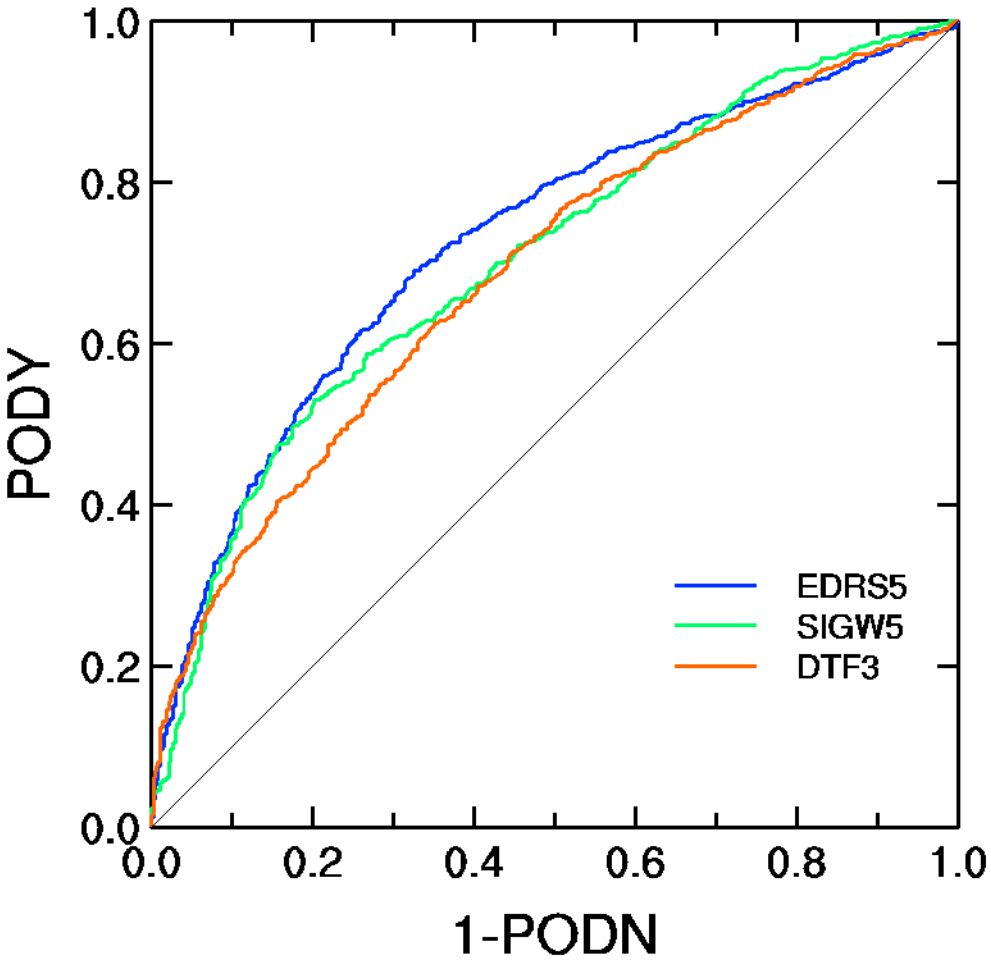

Figure 10. The probability of a (moderate-or-greater) turbulence detection PODY vs the probability of no turbulence PODN from RU20 structure function derived turbulence estimates $\varepsilon^{1/3}$ (blue curve) and σ_w (green curve) compared to the Marroquin TKE diagnostic (orange curve). The case of no skill is also shown as a light diagonal line. The curves are based on 2,141 PIREPs collected at mid-levels (FL100-FL200) over a 3-month winter period.